Journal of
Computational and Theoretical Nanoscience
Vol. 3, 1–7, 2006

Some Recent Progresses in Density-Functional Theory: Efficiency, Accuracy, and Applicability

Chi-Yung Yam, Xiao Zheng, and GuanHua Chen*

Department of Chemistry, The University of Hong Kong, Hong Kong, China

Three new developments of density functional theory are reported here. First, we have developed a highly efficient first-principles method for excited electronic states, whose computational time scales linearly with the system size. Secondly, Neural Networks is introduced to construct the exchange-correlation functional of density functional theory; and lastly, a rigorous first-principles formalism has been established for open electronic systems.

Keywords:

1. INTRODUCTION

Density functional theory (DFT) has become the most popular quantum mechanical method for calculating molecular properties. It has been used to calculate ground and as well as excited state properties of physical, chemical, and biological systems. Despite of its success, DFT has been limited to small and mediate sized systems, and has been mostly applied to isolated systems. Although it is often qualitatively correct, the calculated results of DFT are still not quantitatively accurate enough to make reliable predictions. In this report, we discuss three recent develoments concerning the efficiency, accuracy, and application to open systems for DFT.

2. LINEAR-SCALING TIME-DEPENDENT DENSITY-FUNCTIONAL THEORY

Time-dependent density-functional theory (TDDFT)[1–6] has become a powerful tool to calculate the excited state properties of molecules, such as polarizabilities, hyperpolarizabilities, and excited state energies. It is based on the Runge-Gross theorem[7] which is the time-dependent generalization of the Hohenberg-Kohn theorem.[8,9] The state-of-the-art TDDFT calculations scale as $O(N^3)$[1,10] (N is the number of atoms) which makes the TDDFT a relatively expensive numerical method. Currently the TDDFT calculations are limited to molecules of modest sizes. It is thus desirable to have linear-scaling TDDFT whose computational time scales as $O(N)$.

Much progress has been made for linear-scaling density-functional theory (DFT).[11–16] The bottlenecks for achieving linear-scaling were the calculation of two-electron Coulomb integrals and exchange-correlation (XC) quadratures, and the Hamiltonian diagonalization. The fast multipole method (FMM),[17–20] which was originally developed to evaluate the Coulomb interactions of point charges, led to the linear-scaling computation of the two-electron Coulomb integrals. Linear-scaling evaluation of the XC quadratures was also achieved by exploiting the localized nature of XC potential and by employing the integral pre-screening technique.[15,21] These works pave the way for linear-scaling TDDFT methods.

The remaining obstacle for linear-scaling TDDFT method lies in solving the TDDFT equation. The TDDFT equation is very similar to the time-dependent Hartree-Fock (TDHF) equation. The localized-density-matrix (LDM) method was developed to solve the TDHF equation, and its computational time scales linearly with the system size.[22] Instead of the many-body wave function, the LDM method solves for ρ of a molecular system from which its electronic excited state properties are evaluated. The equation-of-motion (EOM) of ρ is integrated in the time-domain. The linear-scaling of computational time versus the system size is ensured by the introduction of density matrix ρ cutoffs.[22,23] Since TDDFT and TDHF have similar EOMs for ρ, we combine the TDDFT and LDM methods just as TDHF-LDM method.[22] The resulting TDDFT-LDM method shall thus be a linear-scaling method for electronic excited states.

To demonstrate that the TDDFT-LDM method is indeed a linear-scaling method, we have carried calculations on a series of linear alkanes. The accuracy of calculation is determined by the values of l_0 and l_1. For simplicity, we choose $l_0 = l_1 = l = 25$ Å in our calculation. In Figure 1, we examine the $O(N)$ scaling of computational time and

*Author to whom correspondence should be addressed.

RESEARCH ARTICLE

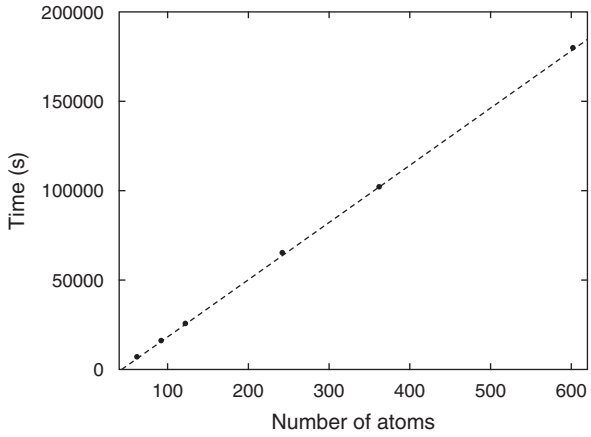

Fig. 1. CPU time for $N = 62, 92, 122, 242, 362, 602$. Each calculation is performed during the time interval between -0.5 fs and 0.5 fs with time step 0.005 fs. $l = 25$ Å is used. Filled circles are the computational times for different sizes and the dashed line is the linear fit to the circles.

plot the CPU time versus N. The computational time spent in solving the DFT ground state is negligible compared to the total CPU time for TDDFT calculation. Clearly, the CPU time scales linearly with N for N between 62 and 602.

We have developed a linear-scaling TDDFT method. The key for our linear-scaling TDDFT method are
(1) solving the TDDFT equation in the time-domain, and
(2) introducing the reduced single-electron density matrix cutoffs.

In addition, the FMM is employed to reduce the computational time for evaluating the Coulomb interaction between the induced and ground state charge distributions. The calculations on the linear alkanes demonstrate the accuracy and efficiency of TDDFT-LDM method. This makes it possible the first-principles calculation of the excited state properties of very large molecular systems.

3. NEURAL NETWORKS BASED EXCHANGE-CORRELATION FUNCTIONAL

Density functional theory (DFT) converts many-electron problems into effective one-electron problems. This conversion is rigorous if the exact exchange-correlation functional is known. It is thus important to find the accurate DFT exchange-correlation functionals, if not exact. Much progress has been made, primarily due to the development of generalized gradient approximation (GGA)[24–26] and hybrid functionals.[27] Various existing exchange-correlation functionals include local or nearly local contributions such as local spin density approximation (LSDA) and generalized gradient approximation (GGA), and nonlocal terms, for instance, exact exchange functional. Although these local and nonlocal exchange and correlation functionals account for the bulk contributions to exact exchange-correlation functional, higher-order contributions are yet to be identified and taken into account. Conceding that it is exceedingly difficult to derive analytically the exact universal exchange-correlation functional, we resort to an entirely different approach.

Since its beginning in the late fifties, Neural Networks has been applied to various engineering problems, such as robotics, pattern recognition, and speech.[28] A neural network is a highly nonlinear system, and is suitable to determine or mimic the complex relationships among relevant physical variables. In this work, we develop a Neural-Networks-based approach to construct the DFT exchange-correlation functional and apply it to improve the results of the popular B3LYP calculations.

B3LYP functional is a hybrid functional composed of several local and nonlocal exchange and correlation contributions, and can be expressed as

$$E_{XC} = a_0 E_X^{\text{Slater}} + (1-a_0)E_X^{\text{HF}} + a_X \Delta E_X^{\text{Becke}} + a_C E_C^{\text{LYP}} + (1-a_C)E_C^{\text{VMN}} \quad (1)$$

where E_X^{Slater} is the local spin density exchange functional,[8, 9, 29] E_X^{HF} is the exact exchange functional, E_X^{Becke} is Becke's gradient-corrected exchange functional,[24] E_C^{LYP} is the correlation functional of Lee, Yang, and Parr,[25] and E_C^{VMN} represents the correlation functional proposed by Vosko, Wilk, and Nusair 30. The values of its three parameters, a_0, a_X, and a_C, dictate the contributions of various terms. They have been determined via the least-square fit to the 116 atomization energies (AEs), ionization potentials (IPs), proton affinities (PAs) and total atomic energies (TAEs) by Becke,[27] and were determined as 0.80, 0.72, and 0.81, respectively. Note that $a_X < a_0 < a_C$. B3LYP functional explicitly consists of the first and second rungs of the Jacob's ladders of density functional approximation[31] and the partial exact exchange functional.[27] Being determined via the least-square fit to the 116 experimental data, B3LYP functional includes implicitly the high-order contribution to the exact functional such as those in the meta-GGA functional.[31] These high-order contributions are averaged over the 116 energy data,[27] and are assumed invariant for all types of atomic or molecular systems. However, their contributions to the exact exchange-correlation energy are in fact system-dependent, which leads to the system-dependence of a_0, a_X, and a_C. After identifying these characteristic properties that are related to the high-order contribution to the exchange-correlation functional, we employ Neural Networks to determine their quantitative relationships to a_0, a_X, and a_C. Instead of being taken as a system-dependent semiempirical functional, the resulting neural network can be viewed as a generalized universal exchange-correlation functional. It can be systematically improved upon the availability of new experimental data. The system-dependence is determined by the characteristic properties of the system. The challenge is to identify these characteristic properties, and more importantly, to determine their quantitative

relationships to the values of a_0, a_X, and a_C. These characteristic properties satisfy two criteria:
(1) they must be of purely electronic nature, since the exact exchange-correlation functional is a universal functional of electron density only; and
(2) they should reflect the electron distribution or its variation.

These properties are termed as the physical descriptors of the electronic system. Beyond the GGA, Perdew, and coworkers[32] proposed the meta-GGA in which the exchange-correlation functional depends explicitly on the kinetic energy density of the occupied Kohn-Sham orbitals,

$$\tau(\mathbf{r}) = \frac{1}{2}\sum_{\alpha}^{\text{occ}} |\nabla\psi_\alpha(\mathbf{r})|^2 \qquad (2)$$

where $\psi_\alpha(\mathbf{r})$ is the wave function of an occupied Kohn-Sham orbital α. The total kinetic energy of the electronic system, $\mathcal{T} = \int \tau(\mathbf{r}) d^3\mathbf{r}$, should relate closely to the high-order corrections to B3LYP functional, and is thus chosen as one of the key descriptors. The exchange-correlation functional is uniquely determined by the electron density distribution $\rho(\mathbf{r})$. $\rho(\mathbf{r})$ can be expanded in terms of the multipole moments. Being the zeroth-order term of the expansion, the total number of electrons N_t is recognized as a natural physical descriptor, and the dipole and quadrupole moments of the system are selected as other descriptors to account for high-order contributions. We use the magnitude of the dipole moment $D \equiv \sqrt{d_x^2 + d_y^2 + d_z^2}$ for the dipole descriptor, where d_i $(i = x, y, z)$ is a component of the dipole vector. For quadrupole descriptor, we take $Q \equiv \sqrt{Q_{xx}^2 + Q_{yy}^2 + Q_{zz}^2}$, where Q_{ii} $(i = x, y, z)$ is a quadrupole moment. The exchange functional accounts for the exchange interaction among the electrons of the same spin. Spin multiplicity g_S is thus adopted as a physical descriptor as well.

Our neural network adopts a three-layer architecture which consists of an input layer, a hidden layer and an output layer.[28] The values of the physical descriptors, g_S, N_t, D, $\mathcal{T}$, and Q are inputed into the neural network at the input layer. The modified values for a_0, a_X, and a_C for each atom or molecule, denoted by $\tilde{a_0}$, $\tilde{a_X}$, and $\tilde{a_C}$, are obtained at the output layer. Different layers are connected via the synaptic weights.[28] The neural network structure such as the number of hidden neurons at the hidden layer is to be determined.

We take the 116 experimental energies that were employed by Becke[27] as our training set, and they are utilized to determine the structure of our neural network and its synaptic weights. Instead of the basis-set-free calculations carried out by Becke,[27] we adopt a Gaussian-type-function (GTF) basis set, 6-311 + $sG(3df, 2p)$, in our calculations. Geometry of every molecule is optimized directly using B3LYP/6-311 + $G(3df, 2p)$. The values of $\mathcal{T}$, D, and Q are obtained at the same level of calculations. Besides g_S, N_t, D, $\mathcal{T}$, and Q, a bias is introduced as another input and its value is set to 1 in all cases. The output values for $\tilde{a_0}$, $\tilde{a_X}$, and $\tilde{a_C}$ vary from system to system, and are used to modify the B3LYP functional for each atom or molecule. The modified B3LYP functional is subsequently used to evaluate its AE, IP, PA, or TAE. The resulting energies are then compared to their experimental values, and the comparison is used to tune the synaptic weights of our neural network. The process is iterated until the differences between the calculated and measured energies are small enough for all the molecules or atoms in the training set, and the neural network is then considered as converged.

Conventional B3LYP/6-311 + $G(3df, 2p)$ calculations are carried out to evaluate AE, IP, PA, or TAE in the training set. Compared to the experimental data, the RMS deviations are 3.0, 4.9, 1.6, and 10.3 kcal/mol for AE, IP, PA, and TAE, respectively. The physical descriptors of each molecule or atom in the training set are inputted to the neural network, and the outputed $\tilde{a_0}$, $\tilde{a_X}$, and $\tilde{a_C}$ are used to construct the B3LYP functional to calculate subsequently AE, IP, PA, or TAE. These values are then compared to the 116 energy values in the training set to tune the values of synaptic weights $\{W_{ji}\}$ and $\{W'_{kj}\}$. It is found that the optimal values of $\tilde{a_0}$, $\tilde{a_X}$, and $\tilde{a_C}$ for each molecule or atom are overall shifted from their origal B3LYP values, although the order $\tilde{a_X} < \tilde{a_0} < \tilde{a_C}$ is kept for each molecule or atom. This overall shift may be caused by the finite basis set. More importantly, their values are slightly different from each other. Therefore, the resulting B3LYP functional is system-dependent. We compare the Neural-Networks-corrected AEs, IPs, PAs, and TAEs to their experimental counterparts. The RMS deviations of Neural-Networks-based B3LYP/6-311 + $G(3df, 2p)$ calculations are 2.8, 3.8, 1.6, and 4.1 kcal/mol, respectively, less than those of the conventional B3LYP/6-311 + $G(3df, 2p)$ calculations, which are 3.0, 4.9, 1.6, and 10.3 kcal/mol for AE, IP, PA, and TAE, respectively. We note that the Neural-Networks-corrected B3LYP/6-311 + $G(3df, 2p)$ calculations yield much improved TAE results. In Becke's original work, the RMS deviations are 2.9, 3.9, 1.9, and 4.1 kcal/mol for AE, IP, PA, and TAE, respectively.

To examine the performance of our neural network, a test is carried out to calculate the IPs of 24 molecules which are selected from the G2 test set.[33] To save the computational time, only 24 small molecules are selected besides those in the training set. Descriptors of each molecule in the testing set are inputed to our neural network and the Neural-Networks-corrected $\tilde{a_0}$, $\tilde{a_X}$, and $\tilde{a_C}$ are used to construct the improved B3LYP functional (see Table I). To calculate their IPs, the cation counterparts of the 24 molecules need to be included as well. Their $\tilde{a_0}$, $\tilde{a_X}$, and $\tilde{a_C}$ are also listed in Table I. The resulting IP values are compared to those obtained from the conventional B3LYP/6-311 + $G(3df, 2p)$ calculations. Except for a few molecules, the resulting IPs for most molecules are improved upon the Neural-Networks correction. For

Table I. Descriptors and parameters of testing set.

Name	g_S	Nt	D (DB)	$\mathcal{T}$ (a.u.)	Q (DB·Å)	$\tilde{a_0}$	$\tilde{a_X}$	$\tilde{a_C}$
CF_2	1	24	0.51	301.68	27.87	0.778	0.748	0.931
CH_2	3	8	0.63	45.13	12.98	0.774	0.751	0.953
CH_2S	1	24	1.75	481.58	33.56	0.778	0.748	0.931
CH_3Cl	1	26	1.96	549.86	33.85	0.780	0.751	0.933
CH_3F	1	18	1.87	176.46	21.21	0.769	0.737	0.927
CH_3	2	9	0.00	49.28	13.87	0.771	0.745	0.947
CH_3OH	1	18	1.67	155.45	22.90	0.769	0.737	0.927
CH_3O	2	17	2.11	149.00	22.23	0.789	0.767	0.954
CHO	2	15	1.69	140.01	19.87	0.785	0.762	0.952
CO_2	1	22	0.00	246.26	28.71	0.775	0.744	0.930
COS	1	30	0.85	589.92	41.32	0.784	0.755	0.934
HOF	1	18	1.95	208.68	17.89	0.769	0.737	0.927
NH_2	2	9	1.83	63.22	12.11	0.771	0.745	0.947
NH	3	8	1.54	58.63	10.94	0.774	0.751	0.953
SC	1	22	1.92	468.67	33.28	0.775	0.744	0.930
B_2H_4	1	14	0.79	76.44	26.08	0.761	0.726	0.923
C_2H_5	2	17	0.34	115.61	25.37	0.789	0.767	0.954
CH_3SH	1	26	1.54	494.06	36.34	0.780	0.751	0.933
CS_2	1	38	0.00	942.06	53.04	0.789	0.761	0.937
N_2H_2	1	16	0.00	142.57	21.13	0.765	0.732	0.925
N_2H_3	2	17	2.56	147.28	21.96	0.789	0.767	0.954
Si_2H_2	1	30	0.57	643.83	50.42	0.784	0.755	0.934
Si_2H_4	1	32	0.00	658.51	51.48	0.786	0.757	0.935
SiH_3	2	17	0.07	306.32	27.95	0.789	0.767	0.954
CF_2^+	2	23	1.08	303.37	20.16	0.798	0.777	0.957
CH_2^+	2	7	0.52	44.66	7.41	0.765	0.739	0.945
CH_2S^+	2	23	1.70	481.65	24.05	0.798	0.777	0.957
CH_3Cl^+	2	25	1.89	550.53	24.57	0.800	0.780	0.958
CH_3F^+	2	17	3.72	177.34	13.46	0.789	0.767	0.954
CH_3^+	1	8	0.00	48.83	7.61	0.745	0.707	0.914
CH_3OH^+	2	17	1.43	155.82	14.56	0.789	0.767	0.954
CH_3O^+	3	16	2.44	149.57	14.24	0.792	0.773	0.959
CHO^+	1	14	3.76	140.98	12.86	0.761	0.726	0.923
CO_2^+	2	21	0.00	245.22	20.89	0.795	0.774	0.956
COS^+	2	29	1.66	588.35	31.06	0.804	0.785	0.959
HOF^+	2	17	2.80	210.63	12.46	0.789	0.767	0.954
NH_2^+	3	8	0.56	62.72	7.39	0.774	0.751	0.953
NH^+	2	7	1.73	58.03	6.69	0.765	0.739	0.945
SC^+	2	21	0.54	469.27	23.22	0.795	0.774	0.956
$B_2H_4^+$	2	13	0.28	75.62	16.76	0.781	0.757	0.951
$C_2H_5^+$	1	16	0.70	117.00	16.11	0.765	0.732	0.925
CH_3SH^+	2	25	1.16	494.52	25.68	0.800	0.780	0.958
CS_2^+	2	37	0.00	941.86	40.10	0.809	0.790	0.960
$N_2H_2^+$	2	15	0.00	143.30	13.30	0.785	0.762	0.952
$N_2H_3^+$	1	16	2.55	148.94	14.25	0.765	0.732	0.925
$Si_2H_2^+$	2	29	0.22	642.41	34.76	0.804	0.785	0.959
$Si_2H_4^+$	2	31	0.00	656.32	36.04	0.805	0.786	0.959
SiH_3^+	2	16	0.06	306.15	17.96	0.787	0.765	0.953

Neural-Networks-based B3LYP/6-311 + $G(3df, 2p)$ calculation, its RMS deviation for the 24 molecules is reduced to 2.4 kcal/mol from the original 3.6 kcal/mol. This test demonstrates the validity of our Neural-Networks-based functional.

4. FIRST-PRINCIPLES METHOD FOR OPEN ELECTRONIC SYSTEMS

Density-functional theory (DFT) has been widely used as a research tool in condensed matter physics, chemistry, materials science, and nanoscience. The Hohenberg-Kohn theorem[8] lays the foundation of DFT. The Kohn-Sham formalism[9] provides a practical solution to calculate the ground state properties of electronic systems. Runge and Gross extended DFT further to calculate the time-dependent properties and hence the excited state properties of any electronic systems.[7] The accuracy of DFT or time-dependent DFT (TDDFT) is determined by the exchange-correlation functional. If the exact exchange-correlation functional were known, the Kohn-Sham formalism would have provided the exact ground state properties, and the Runge-Gross extension, TDDFT, would have yielded the exact properties of excited states. Despite their wide range of applications, DFT and TDDFT have been mostly limited to isolated systems.

Any electron density distribution function $\rho(\mathbf{r})$ of a real physical system is a real analytic function. We may treat nuclei as point charges, and this would only lead to non-analytic electron density at isolated points. In practical quantum mechanical simulations, analytic functions such as Gaussian functions and plane wave functions are adopted as basis sets, which results in analytic electron density distribution. Therefore, we conclude that any electron density functions of real systems are real analytic on connected physical spaces, in principle or in practice. Note that the isolated points at nuclei can be excluded for the moment from the physical space that we consider, so long as the space is connected. Later we will come back to these isolated points, and show that their inclusion does not alter our conclusion. Based on this, we show below that for a real physical system the electron density distribution function in a sub-space determines uniquely its values on the entire physical space. This is nothing but the analytic continuation of a real analytic function. The proof for the univariable real analytical functions can be found in textbooks, for instance, Ref. [43]. The extension to multivariable real analytical functions is straightforward.

Lemma: *The electron density distribution function* $\rho(\mathbf{r})$ *is real analytic in a connected physical space* U. $W \subseteq U$ *is a sub-space. If* $\rho(\mathbf{r})$ *is known for all* $\mathbf{r} \in W$, $\rho(\mathbf{r})$ *can be uniquely determined in entire* U.

We are ready to prove the following theorem.

Theorem: *Electron density function* $\rho(\mathbf{r})$ *for a subsystem of a connected real physical system determines uniquely all electronic properties of the entire system.*

Proof: Assuming the physical space spanned by the subsystem and the connected real physical system are W and U, respectively. W is thus a sub-space of U, i.e., $W \subseteq U$. According to the above lemma, $\rho(\mathbf{r})$ in W determines uniquely its values in U, i.e., $\rho(\mathbf{r})$ of the subsystem determines $\rho(\mathbf{r})$ of the entire system.

Inclusion of isolated points, lines or planes where $\rho(\mathbf{r})$ is non-analytic into the connected physical space

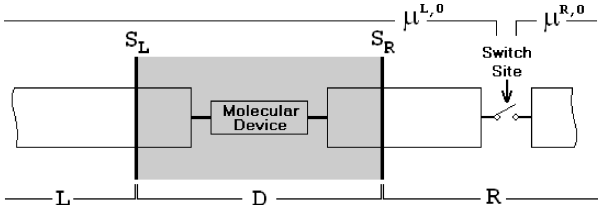

Fig. 2. Schematic representation of the experimental setup for quantum transport through a molecular device.

does not violate the theorem, so long as $\rho(\mathbf{r})$ is continuous at these points, lines or planes. This can be shown clearly by performing analytical continuation of $\rho(\mathbf{r})$ infinitesimally close to them. Therefore, we conclude that $\rho(\mathbf{r})$ of any finite subsystem determines uniquely $\rho(\mathbf{r})$ of the entire physical system including the nuclear sites. Hohenberg-Kohn theorem and Runge-Gross extension state that the electron density distribution of a system determines uniquely all its electronic properties. Therefore, we conclude that $\rho(\mathbf{r})$ for a subsystem determines all the electronic properties of the real physical system.

The above theorem guarantees the existence of an exact DFT-type method for open systems. In principle, all we need to know is the electron density of the reduced system. The electron density distribution in the environment can be obtained by the analytic continuation of the electron density function at or near the boundary. Although in principle its physical span can be extremely small, in practice the reduced system must be chosen appropriately so that this analytic continuation procedure can be carried out. For instance, Figure 2 depicts a molecular device, consisting of a reduced system or device region D, and its environment, the left and right leads L and R. Note that the reduced system D contains not only the molecular device itself, but also portions of the left and right electrodes. In this way the analytic continuation of the density function into the electrodes can be performed readily.

Now the challenge is to develop a practical first-principles method. Taking the molecular device in Figure 2 as an example, we develop an exact DFT formalism for the open systems. To calculate the properties of the molecular device, we need only the electron density distribution in the device region. The influence of the electrodes can be determined by the electron density distribution in the device region D. Within the TDDFT formalism, a closed equation of motion (EOM) has been derived for the reduced single-electron density matrix $\sigma(t)$ of the entire system:[44]

$$i\dot{\sigma}(t) = [h(t), \sigma(t)] \tag{3}$$

where $h(t)$ is the Kohn-Sham Fock matrix, and the square bracket on the right-hand side (RHS) denotes a commutator. The matrix element of σ is defined as $\sigma_{ij}(t) = \langle a_j^\dagger(t)\, a_i(t)\rangle$, where $a_i(t)$ and $a_j^\dagger(t)$ are the Heisenberg annihilation and creation operators for atomic orbitals i and j at time t, respectively. Expanded in a real space basis set, the matrix representation of σ can be partitioned as

$$\sigma = \begin{bmatrix} \sigma_L & \sigma_{LD} & \sigma_{LR} \\ \sigma_{DL} & \sigma_D & \sigma_{DR} \\ \sigma_{RL} & \sigma_{RD} & \sigma_R \end{bmatrix} \tag{4}$$

where σ_L, σ_R, and σ_D represent the diagonal blocks which correspond to the left lead L, the right lead R and the device region D, respectively; σ_{LD} is the off-diagonal block between L and D; and σ_{RD}, σ_{LR}, σ_{DL}, σ_{DR}, and σ_{RL} are similarly defined. The Kohn-Sham Fock matrix h can be partitioned in the same way with σ replaced by h in Eq. (4). Thus, the EOM for σ_D can be written as

$$\begin{aligned} i\dot{\sigma}_D &= [h_D, \sigma_D] + \sum_{\alpha=L,R} (h_{D\alpha}\sigma_{\alpha D} - \sigma_{D\alpha}h_{\alpha D}) \\ &= [h_D, \sigma_D] - i\sum_{\alpha=L,R} Q_\alpha \end{aligned} \tag{5}$$

where Q_L (Q_R) is the dissipative term due to L (R). With the reduced system D and the leads L/R spanned respectively by the atomic orbitals $\{l\}$ and the single-electron states $\{k_\alpha\}$, Eq. (5) is equivalent to:

$$i\dot{\sigma}_{nm} = \sum_{l\in D}(h_{nl}\sigma_{lm} - \sigma_{nl}h_{lm}) - i\sum_{\alpha=L,R} Q_{\alpha,nm} \tag{6}$$

$$Q_{\alpha,nm} = i\sum_{k_\alpha\in\alpha}\left(h_{nk_\alpha}\sigma_{k_\alpha m} - \sigma_{nk_\alpha}h_{k_\alpha m}\right) \tag{7}$$

where h_{nk_α} is the coupling matrix element between the atomic orbital n and the single-electron state k_α. $\sigma_{k_\alpha m}$ is precisely the lesser Green's function of identical time variables, i.e., $\sigma_{k_\alpha m}(t) = -iG^<_{k_\alpha m}(t,t')|_{t'=t}$. Based on the Keldysh formalism[45] and the analytic continuation rules of Langreth,[46] $Q_{\alpha,nm}(t)$ can be calculated by the NEGF formulation as described in Ref. [47],

$$\begin{aligned} Q_{\alpha,nm}(t) = -\sum_{l\in D}\int_{-\infty}^{\infty} d\tau \Big[& G^<_{nl}(t,\tau)\Sigma^a_{\alpha,lm}(\tau,t) \\ & + G^r_{nl}(t,\tau)\Sigma^<_{\alpha,lm}(\tau,t) - \Sigma^<_{\alpha,nl}(t,\tau)G^a_{lm}(\tau,t) \\ & - \Sigma^r_{\alpha,nl}(t,\tau)G^<_{lm}(\tau,t)\Big] \end{aligned} \tag{8}$$

where G^r, G^a, and $G^<$ are the retarded, advanced and lesser Green's function for the reduced system D, respectively, and Σ^r_α, Σ^a_α, and $\Sigma^<_\alpha$ are the retarded, advanced and lesser self-energies due to the lead α (L or R), respectively.

At first glance Eq. (6) is not self-closed since the dissipative terms Q_α remain unsolved. According to the theorem we proved earlier, all physical quantities are explicit or implicit functionals of the electron density in the reduced system D, $\rho_D(\mathbf{r}, t)$. Q_α is thus also a universal functional of $\rho_D(\mathbf{r}, t)$. Therefore, Eq. (6) can be recast into a formally closed form,

$$i\dot{\sigma}_D = \Big[h_D[\mathbf{r}, t; \rho_D(\mathbf{r}, t)], \sigma_D\Big] - i\sum_{\alpha=L,R} Q_\alpha[\mathbf{r}, t; \rho_D(\mathbf{r}, t)] \tag{9}$$

RESEARCH ARTICLE

Neglecting the second term on the RHS of Eq. (9) leads to the conventional TDDFT formulation in terms of reduced single-electron density matrix.[44] The second term describes the dissipative processes where electrons enter and leave the reduced system D. Besides the exchange-correlation functional, an additional universal density functional, the dissipation functional $Q_\alpha[\mathbf{r}, t; \rho_D(\mathbf{r}, t)]$, is introduced to account for the dissipative interaction between the reduced system and its environment. Eq. (9) is thus the TDDFT EOM for the open system. In the frozen DFT approach[49] an additional exchange-correlation functional term was introduced to account for the exchange-correlation interaction between the system and the environment. This additional term is included in $h[\mathbf{r}, t; \rho_D(\mathbf{r}, t)]$ of Eq. (9).

Admittedly $Q_\alpha[\mathbf{r}, t; \rho_D(\mathbf{r}, t)]$ is an extremely complex functional and difficult to evaluate. Just as various approximated expressions have been adopted for the DFT exchange-correlation functional in practical implementations, progressive approximations may be made for Q_α. One such scheme is the adiabatic approximation, which assumes that Q_α at a particular time t_0 depends only on the electron density function ρ_D at the time, i.e.,

$$Q_\alpha[\mathbf{r}, t_0; \rho_D(\mathbf{r}, t)] \approx Q_\alpha^{AD}[\mathbf{r}; \rho_D(\mathbf{r}, t_0)] \qquad (10)$$

where the adiabatic dissipation functional $Q_\alpha^{AD}(\mathbf{r})$ is a functional of the spatial electron density function $\rho_D(\mathbf{r})$ only. The steady-state can be reached adiabatically. Therefore, the steady-state dissipation functional, $Q_\alpha^{SS}[\rho_D(\mathbf{r})]$ is an adiabatic functional, i.e.,

$$Q_\alpha^{SS}[\rho_D(\mathbf{r})] = Q_\alpha^{AD}[\rho_D(\mathbf{r})] \qquad (11)$$

Although its analytical expression is elusive, the numerical evaluation of $Q_\alpha^{SS}[\rho_D(\mathbf{r})]$ can be obtained by using the first-principles NEGF approach in Ref. [38]. In practice, we may obtain the numerical solutions of Q_α^{SS} for a discrete set of steady-state electron density functions, from which we may calculate Q_α^{AD} or Q_α^{SS} for any electron density function by extrapolation.

We have developed an exact TDDFT formalism for open electronic systems by introducing a new dissipation functional, and have proposed two practical schemes to evaluate of the new functional. This work greatly extends the applicability of the density-functional theory.

Acknowledgment: Authors would thank Fan Wang, XiuJun Wang, LiHong Hu, and Yang Zhao for stimulating discussions. Support from the Hong Kong Research Grant Council (HKU 7010/03P) is gratefully acknowledged.

References

1. M. E. Casida, in *Recent Developments and Applications of Modern Density Functional Theory*. edited by J. M. Seminario, Theoretical and Computational Chemistry Elsevier Science, Amsterdam **(1996)**, Vol. 4.
2. S. M. Colwell, N. C. Handy, and A. M. Lee, *Phys. Rev. A* 53, 1316 **(1996)**.
3. V. Chernyak and S. Mukamel, *J. Chem. Phys.* 112, 3572 **(2000)**.
4. M. J. Stott and E. Zaremba, *Phys. Rev. A* 21, 12 **(1980)**.
5. A. Zangwill and P. Soven, *Phys. Rev. Lett.* 45, 204 **(1980)**.
6. G. D. Mahan, *Phys. Rev. A* 22, 1780 **(1980)**.
7. E. Runge and E. K. U. Gross, *Phys. Rev. Lett.* 52, 997 **(1984)**.
8. P. Hohenberg and W. Kohn, *Phys. Rev.* 136, B864 **(1964)**.
9. W. Kohn and L. J. Sham, *Phys. Rev.* 140, A1133 **(1965)**.
10. S. J. A. van Gisbergen, J. G. Snijders, and E. J. Baerends, *J. Chem. Phys.* 103, 9347 **(1995)**.
11. S. Goedecker, *Rev. Mod. Phys.* 71, 1085 **(1999)**.
12. W. Yang, *Phys. Rev. Lett.* 66, 1438 **(1991)**.
13. W. Kohn, *Phys. Rev. Lett.* 76, 3168 **(1996)**.
14. J. M. Millam and G. E. Scuseria, *J. Chem. Phys.* 106, 5569 **(1997)**.
15. G. E. Scuseria, *J. Phys. Chem. A* 103, 4782 **(1999)**.
16. C. F. Guerra, J. G. Snijders, G. te Velde, and E. J. Baerends, *Theor. Chem. Acc.* 99, 391 **(1998)**.
17. L. Greengrad, *Science* 265, 909 **(1994)**.
18. H. Q. Ding, N. Karasawa, and W. A. Goddard III, *J. Chem. Phys.* 97, 4309 **(1992)**.
19. C. A. White, B. G. Johnson, P. M. W. Gill, and M. Head-Gordon, *Chem. Phys. Lett.* 253, 268 **(1996)**; C. A. White, B. G. Johnson, P. M. W. Gill, and M. Head-Gordon, *Chem. Phys. Lett.* 230, 8 **(1994)**.
20. M. C. Strain, G. E. Scuseria, and M. J. Frisch, *Science* 271, 51 **(1996)**.
21. R. E. Stratmann, G. E. Scuseria, and M. J. Frisch, *Chem. Phys. Lett.* 257, 213 **(1996)**.
22. S. Yokojima and G. H. Chen, *Chem. Phys. Lett.* 292, 379 **(1998)**; S. Yokojima and G. H. Chen, *Phys. Rev. B* 59, 7259 **(1999)**.
23. G. H. Chen and S. Mukamel, *J. Phys. Chem.* 100, 11080 **(1996)**.
24. A. D. Becke, *Phys. Rev. A* 38, 3098 **(1988)**.
25. C. Lee, W. Yang, and R. G. Parr, *Phys. Rev. B* 37, 785 **(1988)**.
26. J. P. Perdew and Y. Wang, *Phys. Rev. B* 45, 13244 **(1992)**.
27. A. D. Becke, *J. Chem. Phys.* 98, 5648 **(1993)**.
28. B. D. Ripley, *Pattern Recognition and Neural Networks*, Cambridge University Press, New York **(1996)**.
29. J. C. Slater, *Quantum Theory of Molecular and Solids: The Self-Consistent Field for Molecular and Solids*, McGram-Hill, New York **(1974)**, Vol. 4.
30. S. H. Vosko, L. Wilk, and M. Nusair, *Canadian J. Phys.* 58, 1200 **(1980)**.
31. J. P. Perdew and K. Schmidt, *Density Functional Theory and its Application to Materials*, Melville, New York **(2001)**, and references therein.
32. J. P. Perdew, S. Kurth, A. Zupan, and P. Blaha, *Phys. Rev. Lett.* 82, 2544 **(1999)**; 82, 5179 **(1999)**, (E).
33. L. A. Curtiss, K. Raghavachari, P. C. Redfern, V. Rassolov, and J. A. Pople, *J. Chem. Phys.* 109, 7764 **(1998)**.
34. N. D. Lang and Ph. Avouris, *Phys. Rev. Lett.* 84, 358 **(2000)**.
35. J. Heurich, J. C. Cuevas, W. Wenzel, and G. Schön, *Phys. Rev. Lett.* 88, 256803 **(2002)**.
36. C.-K. Wang and Y. Luo, *J. Chem. Phys.* 119, 4923 **(2003)**.
37. N. D. Lang, *Phys. Rev. B* 52, 5335 **(1995)**.
38. J. Taylor, H. Guo, and J. Wang, *Phys. Rev. B* 63, 245407 **(2001)**.
39. S.-H. Ke, H. U. Baranger, and W. Yang, *J. Am. Chem. Soc.* 126, 15897 **(2004)**.
40. W.-Q. Deng, R. P. Muller, and W. A. Goddard III, *J. Am. Chem. Soc.* 126, 13563 **(2004)**.
41. M. Brandbyge et al., *Phys. Rev. B* 65, 165401 **(2002)**.
42. Y. Xue, S. Datta, and M. A. Ratner, *J. Chem. Phys.* 115, 4292 **(2001)**.
43. S. G. Krantz and H. R. Parks, *A Primer of Real Analytic Functions*, Birkhäuser Boston **(2002)**.
44. C. Y. Yam, S. Yokojima, and G. H. Chen, *J. Chem. Phys.* 119, 8794 **(2003)**; *Phys. Rev. B* 68, 153105 **(2003)**.
45. L. V. Keldysh, *JETP* 20, 1018 **(1965)**.

46. D. C. Langreth and P. Nordlander, *Phys. Rev. B* 43, 2541 **(1991)**.
47. A.-P. Jauho, N. S. Wingreen, and Y. Meir, *Phys. Rev. B* 50, 5528 **(1994)**.
48. G. Stefanucci and C.-O. Almbladh, *Europhys. Lett.* 67 (1), 14 **(2004)**.
49. T. A. Wesolowski and A. Warshel, *J. Phys. Chem.* 97, 8050 **(1993)**.
50. S. Datta, *Electronic Transport in Mesoscopic Systems*, Cambridge University Press **(1995)**.
51. R. Landauer, *Philos. Mag.* 21, 863 **(1970)**.

Received: 10 January 2006. Accepted: 1 March 2006.